Catalysis Science & Technology

PAPER

View Article Online
View Journal | View Issue

Cite this: *Catal. Sci. Technol.*, 2020, **10**, 700

Promotion effect of Mg on a post-synthesized Sn-Beta zeolite for the conversion of glucose to methyl lactate†

Xiaomei Yang,[a] Bin Lv,[a] Tianliang Lu,[b] Yunlai Su[a] and Lipeng Zhou*[a]

Received 24th November 2019,
Accepted 19th December 2019

DOI: 10.1039/c9cy02376c

rsc.li/catalysis

Mg-Sn-Beta zeolites with different Mg/Sn molar ratios were prepared from the parent deAl-Beta by a coimpregnation method. The samples were characterized by powder X-ray diffraction (XRD), N_2 physisorption, ultraviolet-visible diffuse reflectance spectroscopy (UV-vis DRS), X-ray photoelectron spectroscopy (XPS), Fourier transform infrared (FT-IR) spectroscopy of the –OH region and probe molecule (pyridine, CD_3CN and $CHCl_3$) adsorption. The results indicate that Mg^{2+} and Sn^{4+} can react with silanol nests and incorporate into the framework of Beta zeolite. Moreover, it is relatively facile to incorporate Sn^{4+} into the framework. The framework metal sites generate Lewis (L) acid sites; however, the L acid strength of the framework Mg^{2+} is weaker than that of framework Sn^{4+}. A small amount of Mg^{2+} interacts with isolated silanols to form extraframework species. Therefore, the introduction of Mg^{2+} results in a significant reduction in silanol defects and an increase in L acidity/basicity of Mg-Sn-Beta. Mg-Sn-Beta with Mg/Sn molar ratio of 1 has the least silanol defects. In the conversion of glucose to methyl lactate (MLA), Mg-Beta is less active than Sn-Beta due to its weaker L acidity. The TOF value for MLA formation increased in the order of Sn-Beta $<$ 0.25Mg-Sn-Beta $\approx$ 4Mg-Sn-Beta $<$ 1Mg-Sn-Beta, which is closely related to the amount of silanol defects in the catalysts. A kinetic study indicates that the apparent activation energy of the retro-aldol of fructose to MLA, which is the rate-determining step of glucose conversion to MLA, decreases over Mg-Sn-Beta compared to that over Sn-Beta and thus, the formation of MLA was promoted.

1 Introduction

Biomass is an abundant and sustainable resource of the world. Carbohydrates are the main components of plant biomass.[1] Utilizing carbohydrates as raw materials to produce chemicals and biofuels is an important part of sustainable development. Glucose is the most abundant and cheap hexose, which can be produced from inedible cellulose.[2,3] Many high value-added chemicals such as lactic acid (LA) and its derivatives have been produced from glucose.[4] LA and its derivatives have wide applications in the industries of food, cosmetics, pharmaceutical, plastics and chemicals.[5,6] Glucose can be converted to LA in water or alkyl lactate in alcohol by chemocatalytic methods, in addition to microbial fermentation.[5,7] Lewis (L) acids and bases are two kinds of catalysts used for the conversion of glucose to LA or alkyl lactate.[5,7–9] Generally, L acids are more selective than L bases for producing alkyl lactate from hexose in alcohol.

Sn-Beta molecular sieves with strong L acidity and large three-dimensional microporous structure shows excellent performance for transforming carbohydrates to LA and alkyl lactate.[10] However, the selectivity of Sn-Beta for the conversion of hexose to alkyl lactate is affected significantly by its preparation method. Sn-Beta synthesized in fluoride media with fewer silanol defects exhibits higher selectivity for alkyl lactate than the post-synthesized counterpart.[11,12] Unfortunately, the synthesis of Sn-Beta in fluoride media is time-consuming and fluoride is noxious.[13] Post-synthesis methods avoid these drawbacks as Sn-Beta is prepared *via* first the dealumination of Al-Beta to generate vacant T sites and then incorporation of Sn into the vacant T sites.[14] However, the vacant T sites are usually difficult to be completely occupied by Sn, which leads to more silanol defects in the post-synthesized Sn-Beta (Sn-Beta-P), and thus lower selectivity in the conversion of hexose to alkyl lactate. Vega-Vila *et al.* adopted a method involving the reflux of vacuum-dried deAl-Beta and anhydrous $SnCl_4$ in moisture-free dichloromethane to prepare Sn-Beta.[15] The method can

---

[a] *Green Catalysis Center and College of Chemistry, Zhengzhou University, 100 Kexue Road, Zhengzhou 450001, China. E-mail: zhoulipeng@zzu.edu.cn; Tel: +86 371 67781780*
[b] *School of Chemical Engineering, Zhengzhou University, 100 Kexue Road, Zhengzhou 450001, China*

† Electronic supplementary information (ESI) available. See DOI: 10.1039/c9cy02376c

precisely control the density of framework Sn sites and residual vacancy defects in Sn-Beta, and every framework vacancy can be occupied by Sn. However, this method needs to proceed under anhydrous conditions and noxious organic reagent is used. The addition of a promoter to Sn-Beta can improve its selectivity. For example, Tolborg *et al.* added alkali ions to Sn-Beta-P and improved the yield of methyl lactate (MLA) from 20% to 72% in the conversion of sucrose in methanol.[11] Nevertheless, alkali ions will leach into the reaction solution, affecting the stability and recycling of the catalyst. Dong *et al.* used Zn as a promoter of Sn-Beta-P and increased the yield of LA from 23% to 48% in the conversion of glucose in water.[16] They concluded that the introduction of Zn enhanced the amount of both L acid and base sites; the base sites inhibited side reactions and increased the selectivity of LA. Recently, our group used metal oxides as promoters to improve the selectivity of Sn-Beta-P for the conversion of glucose to MLA;[17] the yield of MLA increased from 25% over Sn-Beta-P to 52% over WO_3-promoted Sn-Beta-P. However, the usage of WO_3 is in large amount, which is harmful to health. Moreover, the problem of WO_3 leaching under the reaction conditions cannot be ignored. Therefore, it is necessary to explore a harmless and stable promoter and also reveal its effects on the properties of Sn-Beta, which is important for establishing the structure–property–performance relationship.

The acidity/basicity of Mg compounds is unique, and depends on the state of Mg. MgO is a basic oxide, while Mg^{2+} in the framework MOF can provide L acidity.[18,19] Additionally, Mg^{2+} in the framework site of silicate molecular sieves can induce strong basicity to the framework oxygen atoms.[20] Thus, Mg-based catalysts are widely used in the conversion of carbohydrates.[21,22] In the present study, Mg was used as a promoter to improve the catalytic performance of Sn-Beta-P in the conversion of glucose to MLA. The state of Mg and Sn and the acidity/basicity of Mg-Sn-Beta were characterized by various techniques. The catalytic performance of Mg-Sn-Beta was investigated in the conversion of glucose to MLA. The promotion effect of Mg^{2+} was also revealed.

2 Experimental section

2.1 Materials

The parent Al-Beta zeolite with Si/Al molar ratio of 13.8 was purchased from Nankai University Catalyst Co. (China). 1,3-Dihydroxyacetone dimer (97%, DHA) was obtained from J & K Scientific Ltd., China. Methyl lactate (MLA) was purchased from TCI Shanghai, China. Glucose monohydrate and $SnCl_4·5H_2O$ were purchased from Tianjin Kermel Chemical Reagent, China. Fructose and mannose were purchased from Aladdin Reagent Co., China. Nitric acid (65–68%), $Mg(NO_3)_2·6H_2O$, methanol and naphthalene were purchased from commercial sources and were analytical grade reagents. All chemicals were used as received without further purification.

2.2 Preparation of Mg-Sn-Beta

The parent Al-Beta zeolite was dealuminated with nitric acid (13 mol L^{-1}, 20 mL g^{-1} zeolite) at 100 °C for 20 h. After filtration and washing with deionized water, until the filtration was near neutral, the dealuminated Beta (deAl-Beta) was dried at 100 °C, overnight. Mg-Sn-Beta was prepared by incipient wetness impregnation of $SnCl_4·5H_2O$ and $Mg(NO_3)_2·6H_2O$ aqueous solutions. The mixture was aged at room temperature overnight, dried at 100 °C, and then calcined at 550 °C for 5 h. These samples were denoted as xMg-Sn-Beta, where x is the molar ratio of Mg/Sn. The value of x is 0.25, 0.5, 1, 2 and 4. The nominal Sn content in xMg-Sn-Beta is 2 wt%. For comparison, Sn-Beta and Mg-Beta were also prepared by the same method; the content of Sn or Mg was identical with that in 1Mg-Sn-Beta.

2.3 Characterization

Powder X-ray diffraction (XRD) patterns were obtained on a PANalytical X'pert PRO instrument with Cu Kα radiation (λ = 0.15418 nm). The tube voltage and tube current were 40 kV and 40 mA, respectively. Crystallinities of the samples were calculated according to the area of the XRD peaks at 2θ of 7.9° and 22.6°. The physisorption of N_2 on the sample was determined on a Quantachrome Autosorb instrument at −196 °C. Samples were degassed for 3 h at 300 °C before N_2 adsorption. Total surface area was calculated using Brunauer–Emmett–Teller (BET) method. Micropore and mesopore distributions were calculated by the Horvath–Kawazoe (HK) method and the Barrett–Joyner–Halenda (BJH) method, respectively. Ultraviolet-visible diffuse reflectance spectra (UV-vis DRS) were recorded with an Agilent Technologies Cary Series UV-vis-NIR spectrophotometer and $BaSO_4$ was used as a reference. X-ray photoelectron spectroscopy (XPS) was measured on an RBD upgraded PHI-5000C ESCA system (PerkinElmer) with Mg Kα radiation ($h\nu$ = 1253.6 eV) operating at 250 W and 14.0 kV. The binding energy of C 1s was used as a reference at 284.6 eV. Fourier transform infrared (FT-IR) spectra of the –OH region and deuterated acetonitrile (CD_3CN), pyridine or $CHCl_3$ adsorption spectra were recorded on a Bruker Tenser II FT-IR spectrometer. The sample was pressed into a self-supporting wafer (~13 mg) and placed into an infrared quartz cell. The wafers were pretreated at 450 °C for 3 h under vacuum. After the cell was cooled to 25 °C, the spectrum of the hydroxyl region was recorded, which was also used as the background for CD_3CN, pyridine or $CHCl_3$ adsorption studies. Subsequently, CD_3CN, pyridine or $CHCl_3$ vapor were introduced into the quartz cell until the adsorption reached saturation. The spectra of CD_3CN or $CHCl_3$ adsorption were obtained under vacuum at 25 °C. For the pyridine FT-IR, the sample was heated to the desired temperature and kept for 0.5 h under vacuum. The spectrum was recorded after the sample was cooled to room temperature.

2.4 Catalytic tests

The conversion of carbohydrates was performed in a stainless steel autoclave (80 mL) with a PTFE liner. Typically, the liner was first loaded with methanol (15 mL) and then, carbohydrates (0.37 g) and catalyst (0.20 g) were added. After the autoclave was sealed, the atmosphere over the solution was flushed four times with N_2 and then, N_2 was charged with pressure of 0.4 MPa. Subsequently, the reactor was heated to the desired temperature at a heating rate of 5 °C min^{-1} and kept at that temperature for a designated time. When the reaction was completed, the reactor was cooled to the ambient temperature in an ice water bath. The reaction mixture was centrifuged and the obtained liquid was collected and adjusted to a constant volume with methanol for GC and HPLC analyses. GC analysis was performed on a Shimadzu GC-2014C equipped with an FID detector and naphthalene was used as the internal standard. LC analysis was performed on a Shimadzu LC-20AT HPLC analysis system equipped with an Aminex HPX-87H column (300 mm × 7.8 mm) and a refractive index detector (RID-10A). H_2SO_4 (5 mmol L^{-1}) was used as the mobile phase under the column temperature of 80 °C and flow rate of 0.6 mL min^{-1}. The carbohydrate conversion and product yield were calculated as follows. All product yields are carbon yields.

$$\text{Carbohydrate conversion} = \frac{\text{moles of carbohydrate reacted}}{\text{moles of starting carbohydrate}} \times 100\%$$

$$\text{Product yield} = \frac{\text{moles of product produced}}{\text{moles of starting carbohydrate}} \times \frac{N'_C}{N_C} \times 100\%$$

where N_C and N'_C are the number of carbon atoms in a carbohydrate molecule and a product molecule, respectively.

3 Results and discussion

3.1 Characterization of Mg-Sn-Beta zeolite

3.1.1 Crystalline phase and texture properties. XRD patterns of the samples are shown in Fig. 1. All the samples exhibit well-defined reflections with a *BEA topology. No diffraction peaks assigned to SnO_2 and MgO are observed, indicating that Sn and Mg species are highly dispersed. The relative crystallinity of the samples is listed in Table 1. The crystallinity of Sn-Beta decreases remarkably compared to that of deAl-Beta, probably due to its corrosion in acidic $SnCl_4$ aqueous solution. In contrast, the crystallinity of Mg-Beta increases compared to that of deAl-Beta, indicating that the structure of deAl-Beta is reconstructed during its preparation in the presence of Mg^{2+}. Alkali and/or alkaline earth metal cations as inorganic structure-directing agents (ISDAs) have been widely studied.[23] Herein, Mg^{2+} probably plays a structure-directing role. The crystallinity of Mg-Sn-Beta increases gradually with the amount of Mg in comparison with Sn-Beta, due to the structure-directing role of Mg^{2+}.

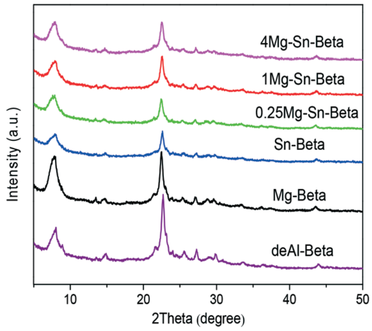

Fig. 1 XRD patterns of deAl-Beta, Mg-Beta, Sn-Beta and Mg-Sn-Beta zeolites.

The results of N_2 physisorption (Table 1 and Fig. 2) show that these samples are microporous materials with a certain amount of mesopores (~9.6 nm) generated through dealumination. The micropore size is in accordance with that of BEA* zeolite.[24] The BET surface area, total pore volume and mesopore volume of Mg-Beta and Sn-Beta decrease slightly when compared with those of deAl-Beta. With the increase in Mg content, these parameters of Mg-Sn-Beta also decrease slightly compared to those of Sn-Beta, except for 4Mg-Sn-Beta. For 4Mg-Sn-Beta, the BET surface area is reduced significantly due to the high content of Mg, implying that there are some Mg species such as small MgO clusters in the pores, leading to the pore blocking to some extent.

3.1.2 State of Mg and Sn in Beta zeolite. UV-vis DR spectra of Mg-Beta, Sn-Beta and Mg-Sn-Beta are shown in Fig. 3. All the zeolites show an absorption band at 200 nm, which is different from that seen for bulk SnO_2 and MgO. For example, SnO_2 exhibits a wide absorption band at the range of 200–300 nm (Fig. S1a†). MgO presents two weak absorption bands at 210 nm and 279 nm (Fig. S1b†). These results indicate that the state of Mg and Sn species in zeolite is different from that in bulk oxide. Probably, Mg and Sn species are located in the framework positions of Beta zeolite, but the presence of extraframework Mg and Sn species is not excluded.

XPS was also conducted to examine the chemical states of Sn and Mg (Fig. 4). In the Sn 3d region (Fig. 4a), two signals positioned at 486.6 and 495.0 eV are observed for SnO_2, which are characteristic of Sn sites of crystalline tin dioxide.[25–27] For Sn-Beta, two bands at higher binding energy (487.7 and 496.2 eV) are found, which are ascribed to $3d_{5/2}$ and $3d_{3/2}$ photoelectrons of tetrahedrally coordinated framework Sn species.[25–27] The binding energy of Sn 3d photoelectrons in 1Mg-Sn-Beta (487.4 and 495.9 eV) is lower than that of Sn-Beta, but it is still much higher than that of SnO_2. This suggests that Sn is incorporated into the framework sites of 1Mg-Sn-Beta. In the Mg 2p region (Fig. 4b), MgO exhibits a narrow peak at 49.3 eV, which is consistent with that reported in the literature.[28] In contrast, Mg 2p peaks for Mg-Beta and 1Mg-Sn-Beta are wide and centered at higher binding energy. This suggests that the chemical state of Mg species in the two samples is nonuniform.

Table 1 Physicochemical properties of deAl-Beta, Mg-Beta, Sn-Beta and Mg-Sn-Beta zeolites

Sample	S_{BET} (m^2 g^{-1})	S_{ex}^{a} (m^2 g^{-1})	V_{tot} (mL g^{-1})	V_{micro} (mL g^{-1})	V_{meso}^{a} (mL g^{-1})	Crystallinity^b (%)	L acid density^c (μmol g^{-1})
Al-Beta	511	154	0.55	0.18	0.37	156	—
deAl-Beta	534	160	0.58	0.19	0.39	100	0
Mg-Beta	513	147	0.51	0.19	0.32	122	34
Sn-Beta	524	177	0.55	0.18	0.37	46	55
0.25Mg-Sn-Beta	515	157	0.51	0.20	0.31	45	85
1Mg-Sn-Beta	515	164	0.54	0.18	0.36	63	83
4Mg-Sn-Beta	480	157	0.52	0.17	0.35	68	111

[a] External surface area = BET surface area − micropore surface area; mesopore volume = total pore volume − micropore volume, where the micropore surface area and volume were determined by the *t*-plot method at a relative pressure of 0.05–0.70. [b] Calculated according to the area of the peaks at 2*θ* of 7.9° and 22.6°. [c] Calculating according to the equation given in the literature.[31]

3.1.3 Acidity and basicity of Mg and/or Sn-Beta zeolites. Fig. 5A shows the FT-IR spectra in the hydroxyl stretching vibration region. The band at the range of 3600–3800 cm^{-1} corresponds to isolated silanols and the band at 3400–3600 cm^{-1} is assigned to silanol nests.[29] Compared to deAl-Beta, the introduction of Mg and/or Sn reduces both the isolated silanols and the silanol nests. It is considered that a metal reacting with silanol nests forms of framework metal sites, while a metal reacting with isolated silanols generates extraframework species. Therefore, both Mg and Sn can be incorporated into the framework of Beta zeolite. Mg^{2+} species interact with silanol nests in two possible ways, as shown in Scheme 1. (1) Mg^{2+} fully incorporated into the framework (species I), resulting in two negative charges that are balanced by one Mg^{2+} cation. (2) Mg^{2+} condensed with two hydroxyl groups of silanol nests (species II). Here, we called this form as quasi-framework Mg species. Zn^{2+} incorporated into the Beta framework was also reported in similar forms.[30] Mg^{2+} interacting with two isolated silanols in the vicinity may form species III, a type of extraframework Mg^{2+} species. The difference spectra of deAl-Beta with Mg-Beta or Sn-Beta are shown in Fig. 5B. It can be seen that Sn incorporation consumes more silanol nests, whereas Mg introduction consumes more isolated silanols. This implies that it is relatively facile to incorporate Sn into the framework sites. Therefore, the amount of the extraframework Mg^{2+} species cannot be ignored. For Mg-Sn-Beta, the amount of silanols decreases first and then increases with the amount of Mg. 1Mg-Sn-Beta has the least silanols. The more silanol defects in 4Mg-Sn-Beta than in 1Mg-Sn-Beta are due to the fact that more small MgO clusters are formed at higher content of Mg, as proved by the results of N_2 physisorption; thus, less Mg^{2+} interacts with silanols.

All coordinatively unsaturated metal sites can serve as L acid sites. CD_3CN is considered to be an efficient and sensitive probe molecule to study framework metal sites and their L acidity.[31,32] FT-IR spectroscopy results of CD_3CN adsorption on the samples is shown in Fig. 6. The absorption

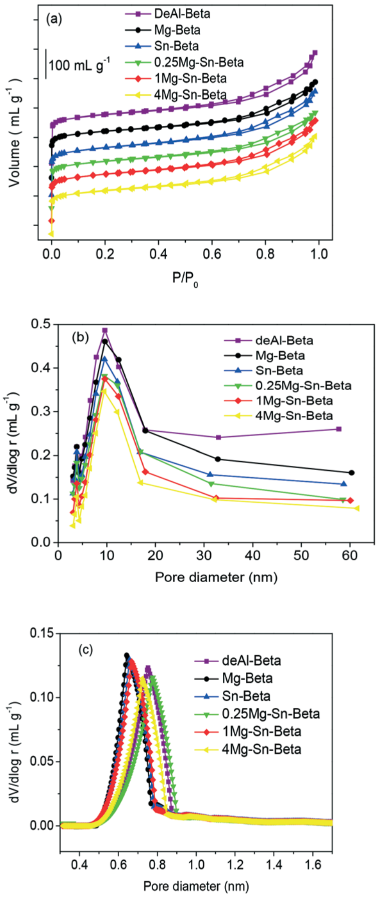

Fig. 2 N_2 adsorption/desorption isotherms (a), BJH (b) and HK (c) derived pore size distributions of the samples.

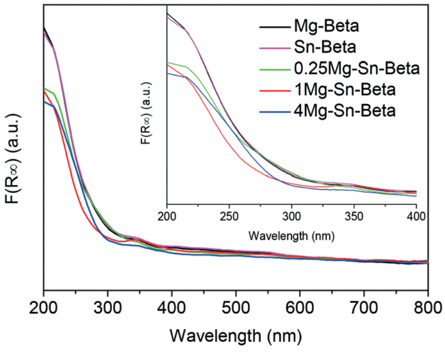

Fig. 3 UV-vis DR spectra of zeolites.

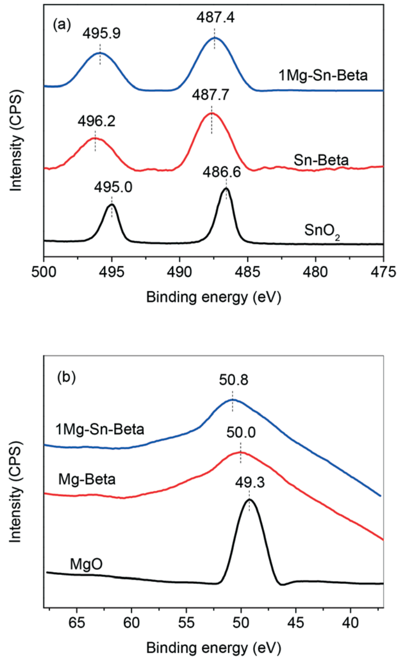

Fig. 4 XPS spectra of Sn 3d (a) in SnO_2, Sn-Beta and 1Mg-Sn-Beta and Mg 2p (b) in MgO, Mg-Beta and 1Mg-Sn-Beta.

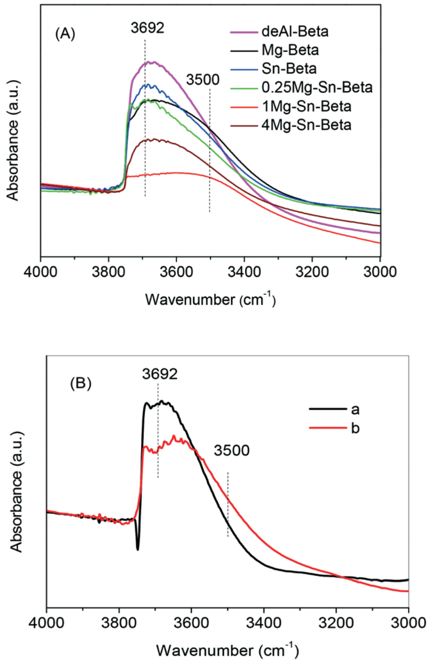

Fig. 5 FT-IR spectra (A) in the hydroxyl stretching vibration region of zeolites and the difference spectra (B) of deAl-Beta with Mg-Beta (a) and Sn-Beta (b).

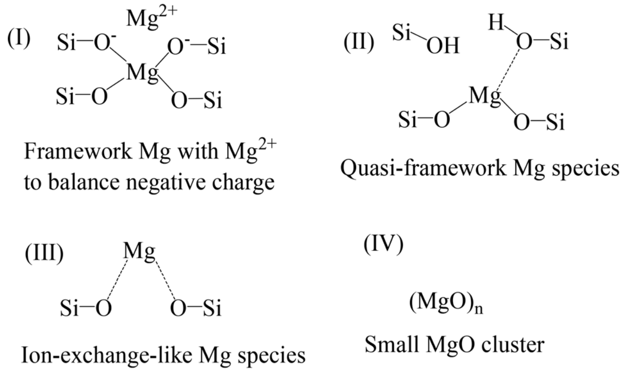

Scheme 1 Possible Mg^{2+} species in Mg-Sn-Beta zeolite.

peak at 2274 cm^{-1} corresponds to CD_3CN adsorbed onto silanols.[27–29,31,32] Besides this peak, Sn-Beta shows another absorption peak at 2310 cm^{-1}, which is assigned to CD_3CN interacting with framework Sn^{4+} sites.[27–29,31,32] Mg^{2+} can form hexa-coordinated compounds such as MgO, so framework Mg^{2+} can also accept electron pairs and act as Lewis acid sites. For Mg-Beta, the peak at 2305 cm^{-1} corresponds to framework Mg^{2+} sites. The lower wavenumber suggests that the L acidity of framework Mg^{2+} sites is weaker than that of framework Sn sites. Mg^{2+} centers as L acid sites are also reported in Mg-MOF-74.[18,19] The intensity of the peak at 2305 cm^{-1} increases with the increase in Mg^{2+} content in Mg-Sn-Beta, indicating that more Mg^{2+} is incorporated into the framework sites to form more L acid sites.

The acidity of Mg-Sn-Beta was also monitored by pyridine adsorption using FT-IR spectroscopy (Fig. 7). DeAl-Beta shows two peaks at 1446 and 1598 cm^{-1}, corresponding to hydrogen-bonded pyridine.[27] For Sn-Beta, two additional peaks at 1452 and 1612 cm^{-1} are also observed, which are ascribed to the vibrations of pyridine adsorbed on L acid sites.[28–30,32,33] For Mg-Beta, these two bands red-shift to 1449 and 1610 cm^{-1}, respectively. This proves again that the L acidity of Mg-Beta is weaker than that of Sn-Beta. On the basis of the area of the peak at 1452 cm^{-1}, the density of L acid sites was calculated and listed in Table 1. It can be seen that the L acid density increases with the increase in Mg content. This is consistent with the results of CD_3CN adsorption. The amount of Brønsted acid sites of all the samples (~1550 cm^{-1}) can be neglected.

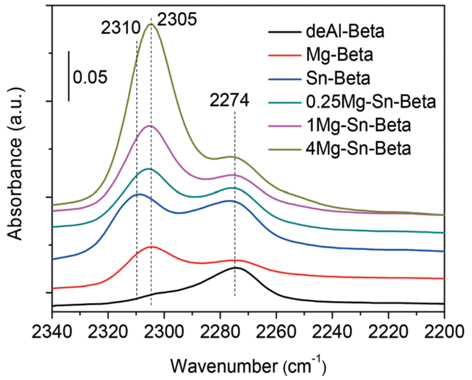

Fig. 6 FT-IR spectra of CD_3CN absorbed on deAl-Beta, Mg-Beta, Sn-Beta and Mg-Sn-Beta. Spectra were obtained at room temperature after desorption for 15 min under vacuum.

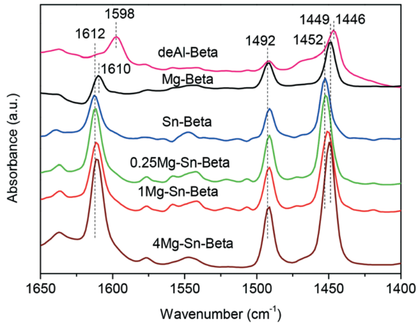

Fig. 7 FT-IR spectra of pyridine adsorbed on different Beta zeolites after evacuation at 150 °C for 30 min.

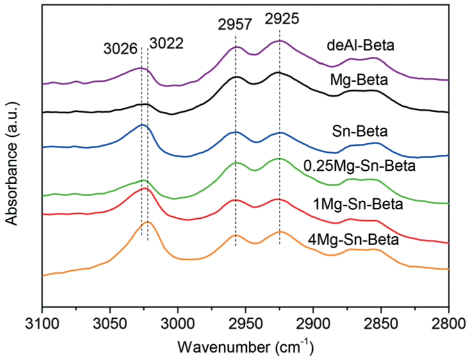

Fig. 8 FT-IR spectra of $CHCl_3$ absorbed on deAl-Beta, Mg-Beta, Sn-Beta and Mg-Sn-Beta. Spectra were obtained at room temperature after desorption for 20 min under vacuum.

The basic properties of the zeolites were examined by recording the FT-IR spectrum of $CHCl_3$-adsorbed samples (Fig. 8). The peak position of the C–H stretching in liquid $CHCl_3$ is at 3033 cm^{-1}.[33,34] This band shifts to lower wavenumbers (3026 cm^{-1}) after $CHCl_3$ adsorbed in the form of species II (Fig. S2†). For 4Mg-Sn-Beta with the highest Mg content, this band shifts to 3022 cm^{-1}. Moreover, the intensity of this band is the highest among these samples, indicating that 4Mg-Sn-Beta has the strongest basicity. The band at 2957 cm^{-1} can be attributed to $CHCl_3$ adsorbed with the mode of species I (Fig. S2†). The weaker the C–H bond, the lower wavenumber of the peak of C–H stretching.[33] Hence, the band at 2925 cm^{-1} is probably caused by $CHCl_3$ adsorbed *via* the mode of species III in Fig. S2.† For all the samples, the intensity of the band at 3026 cm^{-1} decreases, while the intensity of the bands at 2957 cm^{-1} and 2925 cm^{-1} increases with the lapse in desorption time (Fig. S3†). This indicates that the interaction of $CHCl_3$ with zeolite through the modes of species I and III is strong.

3.2 Catalytic performance of Mg-Sn-Beta zeolite

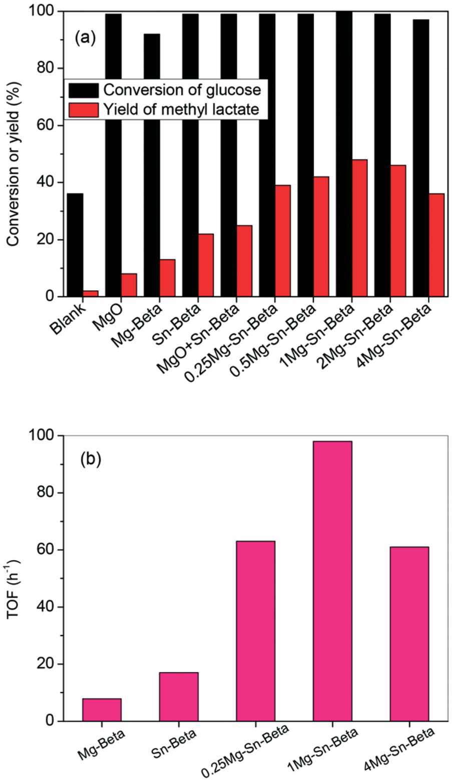

Fig. 9 (a) Conversion of glucose in methanol and (b) TOF (h^{-1}) over various Beta zeolites. Reaction conditions: glucose (0.37 g), catalyst (0.20 g), methanol (15 mL), N_2 (0.4 MPa), (a) 160 °C for 5 h and (b) 140 °C with about 10% MLA yield. The binary catalyst is composed of Sn-Beta (0.20 g) and MgO (0.10 g).

3.2.1 Conversion of glucose to MLA over various catalysts. The catalytic performance of Mg-Sn-Beta was tested in the conversion of glucose to MLA in methanol (Fig. 9). For comparison, Mg-Beta, Sn-Beta and the binary catalyst of MgO and Sn-Beta were also investigated. A negligible yield of MLA was obtained without catalyst, though 36% of glucose was converted. The main product was fructose (17%) that was derived from glucose isomerization. A small amount of erythrose (5%) and glycolaldehyde (4%) derived from retro-aldol of glucose were also detected. In addition, a few other C_3 products (adducts of pyruvaldehyde with methanol, 2%) were also observed. Sn-Beta gives 99% of glucose conversion and 22% of MLA yield. The low MLA yield over the post-synthesized Sn-Beta is expected and is consistent with that reported in the literature.[11,12,17] The conversion of glucose and the yield of MLA over Mg-Beta are lower than those over Sn-Beta, due to the lower L acidity of Mg-Beta. However, Mg-Beta is more selective for the formation of MLA than MgO. Mg-Beta mainly exhibits L acidity, while MgO is a typical solid base. Both the activation mode for the substrate and the formation mechanism of MLA over L acid and base are different.[8,35] L acid generally has higher selectivity than L base for the conversion of carbohydrates to alkyl lactate. Our recent study indicates that the addition of some oxides such as WO_3 as co-catalysts can remarkably improve the selectivity of Sn-Beta for MLA,[17] but MgO as a co-catalyst hardly works. The yield of MLA over the MgO-combined Sn-Beta binary catalyst is similar to that obtained over Sn-Beta alone. It has been revealed that the ultra-small WO_3 particles leached from bulk WO_3 were adsorbed onto the Sn-Beta surface and resulted in the reduction of silanol defects, which contributed to the increase in MLA yield.[17] We measured the leached amount of Mg from MgO during the reaction by the ICP method. Only 0.06 mol% of Mg was leached from MgO, which implies that MgO is much more stable than WO_3 (1.5 mol% of W leached from WO_3). Probably, this is the reason why bulk MgO is an ineffective co-catalyst. In contrast, the yield of MLA increases drastically over Mg-Sn-Beta zeolites. The yield of MLA increases first and then decreases with the content of Mg. The highest MLA yield (48%) is obtained over 1Mg-Sn-Beta. Turnover frequency (TOF) values for MLA formation ($mol_{MLA}\ mol^{-1}{}_{L\ acid\ sites}\ h^{-1}$) from glucose over Mg-Beta, Sn-Beta and Mg-Sn-Beta zeolites were calculated and given in Fig. 9b. The TOF value increases in the order of Mg-Beta < Sn-Beta < 0.25Mg-Sn-Beta ≈ 4Mg-Sn-Beta < 1Mg-Sn-Beta. Mg-Sn-Beta with fewer silanol defects gives higher activity for MLA formation than Sn-Beta. Among Mg-Sn-Beta zeolites, 1Mg-Sn-Beta has the least silanol defects and exhibits the highest activity for MLA formation. The results suggest that the amount of silanol defects plays a crucial role in the conversion of glucose to MLA. The adverse effect of the high-defect environment of Sn-Beta was also observed in the isomerization of glucose to fructose.[15] Probably, the elimination of silanol defects decreased the weak Brønsted acidity, reduced the formation of byproducts and thus improved the selectivity of MLA.[11]

The conversion of glucose to MLA is a reaction with multiple steps mainly including (1) isomerization of glucose to fructose, (2) retro-aldol of fructose to DHA and glyceraldehyde (GLA) and (3) isomerization of DHA and GLA to MLA (Scheme S1†).[10,17] The activity of Mg-Sn-Beta for each step was studied and compared with that of Sn-Beta and Mg-Beta. For the isomerization of glucose in methanol (Table 2), Mg-Beta alone shows low activity. Isomerization of glucose to fructose is catalyzed by a base or L acid.[21,22,29,31] Mg-Beta only exhibits weak L acidity/basicity, so its activity is very low for isomerization of glucose. Sn-Beta was much more active for glucose isomerization to fructose. Glucose is converted quickly at moderate temperature and fructose is the main product. The high activity of Sn-Beta for glucose isomerization originates from the strong L acidity of framework Sn sites, which can form a complex with glucose and complete isomerization *via* 1,2-H-shift.[35] In addition, a certain amount of mannose, an epimer of glucose, was also detected. A small amount of C_3 products including MLA and other C_3 products were also formed, which are the retro-aldol products of fructose. Mg-Sn-Beta is less active and selective than Sn-Beta for glucose isomerization to fructose. It has been proved that open Sn sites with adjacent silanols facilitate glucose isomerization to fructose.[36–38] The decrease in silanol content in Mg-Sn-Beta explains the lower activity and selectivity of Mg-Sn-Beta for isomerization of glucose to fructose. However, the amount of C_3 products increases notably over Mg-Sn-Beta.

The results of fructose conversion over Mg-Beta, Sn-Beta and 1Mg-Sn-Beta are presented in Table 3. The activity of Mg-Beta for the retro-aldol reaction of fructose is very low, and the yield of total C_3 products is only 7% at 140 °C for 1 h. Sn-Beta shows higher activity for the retro-aldol reaction of fructose than Mg-Beta. 20% yield of total C_3 products is achieved at 140 °C for 1 h. For 1Mg-Sn-Beta, the selectivity for the retro-aldol products is much higher than that for Sn-Beta, and 54% of the yield of total C_3 compounds is obtained at 140 °C for 1 h. The TOF values of Mg-Beta, Sn-Beta and 1Mg-Sn-Beta for MLA formation from fructose were calculated based on the amount of L acid sites (Table 3). The TOF values of the above catalysts decrease in the order: 1Mg-Sn-Beta (208 h^{-1}) > Sn-Beta (40 h^{-1}) > Mg-Beta (11 h^{-1}). In addition, the kinetic studies of the retro-aldol reaction of fructose over 1Mg-Sn-Beta were performed and compared with Sn-Beta. The results are given in Fig. S4–S6.† The kinetic data (Fig. S4 and S5†) show that the formation of MLA from the retro-aldol reaction of fructose fitted well with the pseudo-first-order reaction kinetics, which is consistent with our previous report.[12,17] The rate constant of MLA formation over 1Mg-Sn-Beta is larger than that over Sn-Beta at the same temperature, indicating that the formation of MLA is faster over the former. The apparent activation energies over 1Mg-Sn-Beta

Table 2 Isomerization of glucose in methanol[a]

Catalyst	Temp. (°C)	Conv. (%)	Yield (%)			
			Fructose	Mannose	Other C_3	MLA
Mg-Beta	90	6.0	2.2 (33)	0	0	0
	100	7.0	4.4 (57)	0	0	0
	110	10	6.3 (60)	0	0	0
Sn-Beta	80	46	28 (61)	5.1	0	1.1
	90	70	43 (61)	6.8	1.4	1.6
	100	91	53 (58)	6.9	2.6	1.8
	110	97	56 (58)	7.8	2.9	2.6
1Mg-Sn-Beta	80	19	11 (58)	0.7	1.4	1.6
	90	45	18 (40)	3.8	2.1	3.2
	100	60	20 (33)	4.9	4.6	7.3
	110	80	20 (25)	5.3	8.5	19

[a] Reaction conditions: glucose (0.37 g), catalyst (0.20 g), methanol (15 mL), N_2 (0.4 MPa), 1 h. The value in the parenthesis is the selectivity for fructose.

Table 3 Retro-aldol of fructose in methanol[a]

Catalyst	Temp. (°C)	Conv. (%)	Yield (%) MLA	Yield (%) Other C_3	Yield (%) Total C_3	TOF[b] (h^{-1})
Mg-Beta	120	25	1.7	0	1.7	11
	140	39	3.7	3.4	7.1	
Sn-Beta	120	48	1.7	1.3	3.0	40
	140	55	11	8.6	20	
1Mg-Sn-Beta	120	80	26	12	38	208
	140	90	37	17	54	

[a] Reaction conditions: fructose (0.37 g), catalyst (0.20 g), methanol (15 mL), N_2 (0.4 MPa), 1 h. [b] Defined as mole MLA generated per mole L acid sites per hour. The reaction was performed at 140 °C and the yield of MLA was about 10%.

and Sn-Beta were 73 and 119 kJ mol^{-1}, respectively (Fig. S6†). This means that the introduction of magnesium eliminated the proximal silanol of Sn sites, lowered the activation energy and facilitated the formation of MLA. The above results prove that Mg-Sn-Beta significantly promotes the retro-aldol reaction of fructose, which is the rate-determining step of glucose conversion to alkyl lactate.[10] The possible mechanism of the retro-aldol of fructose over Mg-Sn-Beta is given in Scheme 2.

The performance of Mg-Beta, Sn-Beta and Mg-Sn-Beta for the isomerization of DHA to MLA was also investigated (Fig. 10a and b). The activities of the three catalysts follow the order Sn-Beta > Mg-Sn-Beta > Mg-Beta. The conversion of DHA to MLA is also a reaction catalyzed by the L acid.[32,39] However, the L acidity of Mg-Beta is too low to catalyze the conversion of DHA to MLA. The L acidity of Mg-Sn-Beta is higher than that of Sn-Beta, but Mg-Sn-Beta has less silanols, which restrained its activity for the conversion of DHA to MLA.[32]

Based on the above results, it can be concluded that compared to Sn-Beta, Mg-Sn-Beta has a significant promotion effect on the retro-aldol of fructose, which is the rate-determining step of glucose conversion to MLA; therefore, the yield of MLA is improved.

3.2.2 Effect of reaction conditions. Subsequently, the reaction temperature and time were optimized (Fig. 11). The yield of MLA increases with the reaction temperature until 170 °C. Following this, the yield of MLA decreases slightly due to the formation of byproducts, such as humins. The yield of MLA increases with the reaction time and reaches 50% at 170 °C for 5 h. On further prolonging the reaction time, the yield of MLA remains almost unchanged. The yield of MLA from glucose over 1Mg-Sn-Beta (50%) was higher than that over Sn-Beta synthesized in fluoride (43%),[10] which was also higher than that over nanosized Sn-Beta (41%).[27] Moreover, the preparation of Mg-Sn-Beta by the coimpregnation method is relatively simple. In comparison with the alkali ion-modified Sn-Beta catalyst[11] and the binary catalyst of WO_3 and Sn-Beta,[17] Mg species do not easily leach out compared to alkali ions and W species, so Mg-Sn-Beta will be more stable. Mg-Sn-Beta can also transform glucose solutions in high concentrations. As shown in Fig. 11c, 40% of MLA yield is obtained when the concentration of glucose is 12.3 wt% (1.48 g of glucose in 15 mL of methanol), which is higher than that observed over the WO_3-combined Sn-Beta binary catalyst.[17]

3.2.3 Product evolution with reaction time. A time-course study was further conducted at 120 °C to examine the product evolution over Mg-Sn-Beta (Fig. 12). Glucose rapidly isomerizes to fructose and at the same time, a few molecules of mannose, erythrose and glycolaldehyde are also formed. With the time-lapse, the formed fructose is further converted to the C_3 products, including MLA, other C_3 products and a small amount of LA. The total amount of mannose,

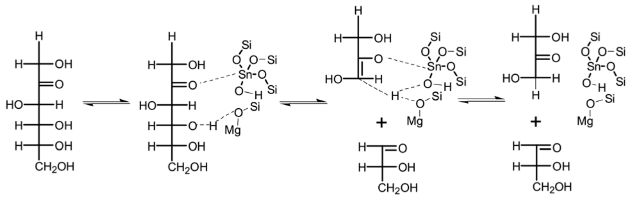

Scheme 2 Proposed mechanism of retro-aldol of fructose over Mg-Sn-Beta.

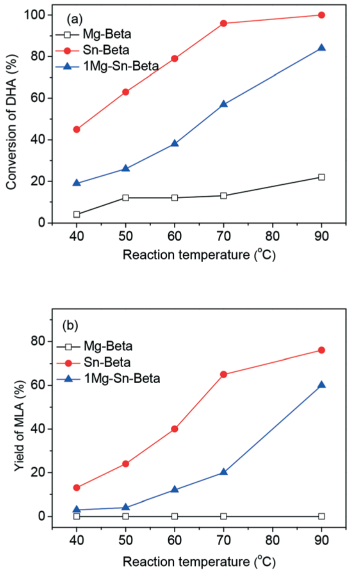

Fig. 10 Isomerization of DHA to MLA over Mg-Beta, Sn-Beta and 1Mg-Sn-Beta. Reaction conditions: DHA (0.37 g), catalyst (0.20 g), methanol (15 mL), N_2 (0.4 MPa), 1 h.

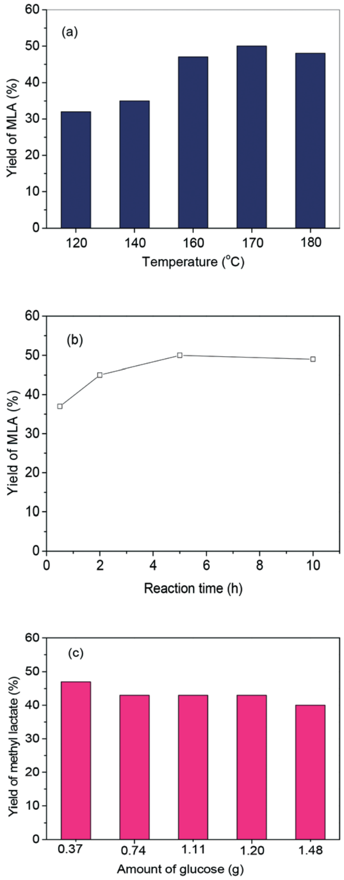

Fig. 11 Effects of reaction temperature (a), time (b) and glucose concentration (c) on the yield of MLA. Reaction conditions: glucose (0.37 g), 1Mg-Sn-Beta (0.20 g), methanol (15 mL), N_2 (0.4 MPa), (a) 5 h, (b) 170 °C and (c) 160 °C for 5 h.

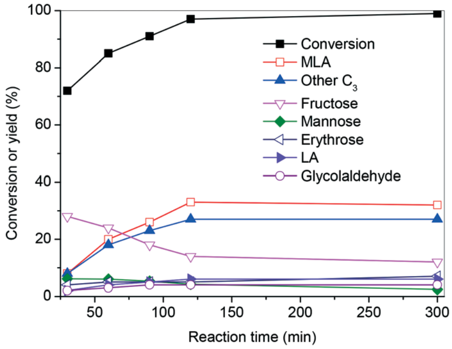

Fig. 12 Conversion of glucose in methanol over Mg-Sn-Beta. Reaction conditions: glucose (0.37 g), 1Mg-Sn-Beta (0.20 g), methanol (15 mL), N_2 (0.4 MPa), 120 °C.

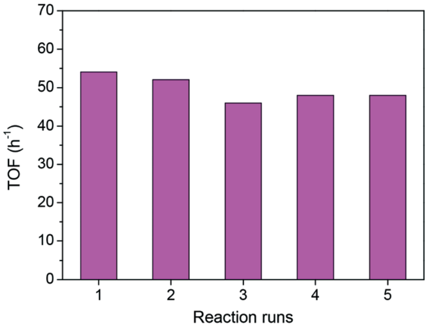

Fig. 13 Reusability of 1Mg-Sn-Beta catalyst. Reaction conditions: glucose (0.37 g), 1Mg-Sn-Beta (0.20 g), methanol (15 mL), N_2 (0.4 MPa), 120 °C, 0.5 h.

erythrose, glycolaldehyde and LA is always low (~5%) during the investigated period. The amount of MLA and other C_3 products kept a similar variation trend. It is found that increasing the temperature promotes the formation of MLA (Fig. 11a), whereas it almost does not affect the formation of other C_3 products (Fig. S7†). This suggests that the formation of MLA and other C_3 products are two competitive reactions and the conversion of other C_3 products to MLA *via* a back reaction is difficult.[40]

3.2.4 Reusability of Mg-Sn-Beta zeolite. Finally, the reusability of 1Mg-Sn-Beta was investigated, which was evaluated according to the initial activity of MLA formation. After each run, the catalyst was recovered by centrifugation, washed with methanol for three times, dried at ambient temperature, calcined at 550 °C for 1 h and then used for the next run. As shown in Fig. 13 and S8,† the TOF value of MLA formation, the conversion of glucose and the yield of MLA only decreased slightly after five runs. The catalyst recovered from the fifth reaction was washed with methanol, dried and calcined at 550 °C for 2 h and then, it was characterized by XRD, N_2 physisorption and ICP analyses (Fig. S9 and Table S1†). The results show that the crystallinity, surface area and pore volume of the reused 1Mg-Sn-Beta decreased slightly after five runs. ICP results show that 2.6% of Sn and 2.0% of Mg were leached from 1Mg-Sn-Beta after five reaction runs, suggesting that Sn and Mg are not facile to leach from the catalyst. These results indicate that the catalyst is stable and recyclable.

Conclusions

Mg-Sn-Beta zeolites with different Mg/Sn molar ratios prepared from deAl-Beta by a coimpregnation method have higher L acidity/basicity and fewer silanol defects than those in Sn-Beta. Both Mg and Sn can be incorporated into the framework sites of Beta zeolite to generate L acid sites, but the L acidity of framework Mg^{2+} is weaker than framework Sn^{4+}. The increase in L basicity results from O^{2-} connected to Mg^{2+}. For the glucose conversion to MLA, Mg-Sn-Beta zeolites promoted the rate-determining step of the retro-aldol of fructose, and thus improved the selectivity of MLA.

Conflicts of interest

There are no conflicts to declare.

Acknowledgements

We are grateful to the National Natural Science Foundation of China (21871236) for the financial support. The program of Young Key Teacher of Universities in Henan Province (2019GGJS015) is also acknowledged.

Notes and references

1 R. A. Sheldon, *ACS Sustainable Chem. Eng.*, 2018, **6**, 4464–4480.

2 M. Yabushita, H. Kobayashi and A. Fukuoka, *Appl. Catal., B*, 2014, **145**, 1–9.

3 L. Zhou, X. Yang, J. Xu, M. Shi, F. Wang, C. Chen and J. Xu, *Green Chem.*, 2015, **17**, 1519–1524.

4 W. Deng, Q. Zhang and Y. Wang, *Catal. Today*, 2014, **234**, 31–41.

5 P. Maki-Arvela, I. L. Simakova, T. Salmi and D. Y. Murzin, *Chem. Rev.*, 2014, **114**, 1909–1971.

6 S. Yamaguchi, M. Yabushita, M. Kim, J. Hirayama, K. Motokura, A. Fukuoka and K. Nakajima, *ACS Sustainable Chem. Eng.*, 2018, **6**, 8113–8117.

7 L. Zhou, L. Wu, H. Li, X. Yang, Y. Su, T. Lu and J. Xu, *J. Mol. Catal. A: Chem.*, 2014, **388–389**, 74–80.

8 Z. Liu, W. Li, C. Pan, P. Chen, H. Lou and X. Zheng, *Catal. Commun.*, 2011, **15**, 82–87.

9 J. Duo, Z. Zhang, G. Yao, Z. Huo and F. Jin, *Catal. Today*, 2016, **263**, 112–116.

10 M. S. Holm, S. Saravanamurugan and E. Taarning, *Science*, 2010, **328**, 602–605.

11 S. Tolborg, I. Sádaba, C. M. Osmundsen, P. Fristrup, M. S. Holm and E. Taarning, *ChemSusChem*, 2015, **8**, 613–617.

12 X. Yang, J. Bian, J. Huang, W. Xin, T. Lu, C. Chen, Y. Su, L. Zhou, F. Wang and J. Xu, *Green Chem.*, 2017, **19**, 692–701.

13 S. Tolborg, A. Katerinopoulou, D. D. Falcone, I. Sádaba, C. M. Osmundsen, R. J. Davis, E. Taarning, P. Fristrup and M. S. Holm, *J. Mater. Chem. A*, 2014, **2**, 20252–20262.

14 P. Y. Dapsens, C. Mondelli and J. Pérez-Ramírez, *Chem. Soc. Rev.*, 2015, **44**, 7025–7043.

15 J. C. Vega-Vila, J. W. Harris and R. Gounder, *J. Catal.*, 2016, **344**, 108–120.

16 W. Dong, Z. Shen, B. Peng, M. Gu, X. Zhou, B. Xiang and Y. Zhang, *Sci. Rep.*, 2016, **6**, 26713.

17 X. Yang, Y. Zhang, L. Zhou, B. Gao, T. Lu, Y. Su and J. Xu, *Food Chem.*, 2019, **289**, 285–291.

18 X. Lu, L. Wang and X. Lu, *Catal. Commun.*, 2018, **110**, 23–27.

19 C. P. Cabello, G. Gûmez-Pozuelo, M. Opanasenko, P. Nachtigall and J. Čejka, *ChemPlusChem*, 2016, **81**, 828–835.

20 Y. Zhou, Y. Jin, M. Wang, W. Zhang, J. Xie, J. Gu, H. Wen, J. Wang and L. Peng, *Chem. – Eur. J.*, 2015, **21**, 15412–15420.

21 I. Delidovich and R. Palkovits, *Catal. Sci. Technol.*, 2014, **4**, 4322–4329.

22 I. Graça, D. Iruretagoyena and D. Chadwick, *Appl. Catal., B*, 2017, **206**, 434–443.

23 J. Shin, D. Jo and S. B. Hong, *Acc. Chem. Res.*, 2019, **52**, 1419–1427.

24 R. Xu, W. Pang and Q. Huo, *Chemistry of Zeolites and Related Porous Materials*, Science Press, Beijing, 2nd edn, 2014, p. 164.

25 G. Zhang, P. Feng, W. Zhang, H. Liu, C. Wang, H. Ma, D. Wang and Z. Tian, *Microporous Mesoporous Mater.*, 2017, **247**, 158–165.

26 B. Tang, W. Dai, G. Wu, N. Guan, L. Li and M. Hunger, *ACS Catal.*, 2014, **4**, 2801–2810.

27 X. Yang, Y. Liu, X. Li, J. Ren, L. Zhou, T. Lu and Y. Su, *ACS Sustainable Chem. Eng.*, 2018, **6**, 8256–8265.

28 J. Chen and J. Zhu, *Res. Chem. Intermed.*, 2019, **45**, 947–950.

29 H. J. Cho, N. S. Gould, V. Vattipalli, S. Sabnis, W. Chaikittisilp, T. Okubo, B. Xu and W. Fan, *Microporous Mesoporous Mater.*, 2019, **278**, 387–396.

30 M. Orazov and M. E. Davis, *Chem. Sci.*, 2016, **7**, 2264–2274.

31 J. W. Harris, M. J. Cordon, J. R. Di Iorio, J. C. Vega-Vila, F. H. Ribeiro and R. Gounder, *J. Catal.*, 2016, **335**, 141–154.

32 X. Yang, L. Wu, Z. Wang, J. Bian, T. Lu, L. Zhou, C. Chen and J. Xu, *Catal. Sci. Technol.*, 2016, **6**, 1757–1763.

33 M. Tamura, K.-i. Shimizu and A. Satsuma, *Appl. Catal., A*, 2012, **433–434**, 135–145.

34 E. Bosch, S. Huber, J. Weitkamp and H. Knözinger, *Phys. Chem. Chem. Phys.*, 1999, **1**, 579–584.

35 Y. Roman-Leshkov, M. Moliner, J. A. Labinger and M. E. Davis, *Angew. Chem., Int. Ed.*, 2010, **49**, 8954–8957.

36 L. Jiang, L. Zhou, J. Chao, H. Zhao, T. Lu, Y. Su, X. Yang and J. Xu, *Appl. Catal., B*, 2018, **220**, 589–596.

37 G. Yang and L. Zhou, *ACS Catal.*, 2018, **8**, 6691–6698.

38 R. Bermejo-Deval, M. Orazov, R. Gounder, S. Hwang and M. E. Davis, *ACS Catal.*, 2014, **4**, 2288–2297.

39 E. Taarning, S. Saravanamurugan, M. S. Holm, J. Xiong, R. M. West and C. H. Christensen, *ChemSusChem*, 2009, **2**, 625–627.

40 R. M. West, M. S. Holm, S. Saravanamurugan, J. Xiong, Z. Beversdorf, E. Taarning and C. H. Christensen, *J. Catal.*, 2010, **269**, 122–130.